MORPHOLOGICAL OPERATORS FOR IMAGES VALUED ON THE SPHERE

Joana Frontera-Pons[1], *Jesus Angulo*[2]

[1]SONDRA Research Alliance, Supélec, France
[2] CMM-Centre de Morphologie Mathématique, Mathématiques et Systèmes, MINES Paristech, France

ABSTRACT

The lack of a natural ordering on the sphere presents an inherent problem when defining morphological operators extended to unit sphere. We analyze here the notion of averaging over the unit sphere to obtain a local origin which can used to formulate ordering based operators. The notion of local supremum and infimum is introduced, which allows to define the dilation and erosion for images valued on the sphere. The algorithms are illustrated using polarimetric images.

Index Terms— mathematical morphology, supremum on sphere, polarimetric image processing

1. INTRODUCTION

Mathematical morphology is a well-known nonlinear approach for image processing [8]. It is based on the calculation of minimum and maximum values of local neighborhoods [10] . Computation of the supremum and infimum of a set of points requires defining an ordering relationship between them. It is obvious that there is no natural ordering on the unit (hyper-)sphere. In fact, the sphere is probably one of the more complex geometrical objects for the notion of ordering and consequently for the computation of rank values such as the supremum/infimum. Mathematical morphology operators were extended to the unit circle [5], however the generalization of such results to the unit (hyper-)sphere is not straightforward. By the way, averaging data on the sphere is also an active research [1, 3].

The values on the unit sphere may represent different kinds of physical information. In imaging applications, the most classical case is the orientation images. In modern medical imaging, High Angular Resolution Imaging (HARDI) produces also images with values on the sphere. Nevertheless the application domain studied is the polarimetric radar data defined on spatial support.

The notion of supremum in vector spaces is usually associated to a marginal computation of maximum coordinates, which involves also a value which has maximal Euclidean distance to the origin [9, 11]. The latter considered as the smallest element of the space. A possible solution to deal with $\mathbb{S}^2$ will consist just in defining a local origin on the sphere and try after projecting on the tangent space, compute a vector-like supremum.

This is the idea which is introduced in this article. The approach induces a partial ordering "adapted" to a particular set of values on the sphere, and it is related to the definition of a barycenter, which allows defining a local Euclidean coordinate system.

2. FRÉCHET - KARCHER BARYCENTER ON $\mathbb{S}^2$

The Fréchet mean is defined as the value minimizing the sum of squared distances along geodesics on Riemannian manifolds [4, 6], i.e., for a given set of points $R = \{\xi_i\}_{i=1}^N$ on the sphere, we have

$$\mu^\circ(R) = \arg\min_{\xi \in \mathbb{S}^2} \sum_{i=1}^{N} d(\xi_i, \xi_k)^2 \tag{1}$$

The problem of computation of the Fréchet mean on the sphere μ° is usually solved using a gradient descent method as proposed by Karcher [6]. Some of the properties of unicity were particulary studied in [1]. The method to estimate the Fréchet mean on a sphere consists first projecting the points $\xi_i \in \mathbb{S}^2$ onto a tangent plane $T_{\mathbf{y}_t}\mathbb{S}^2$ at an initial point $\mathbf{y}_t \in \mathbb{S}^2$ by an inverse projection

$$\vec{\nu}_i = \exp_{\mathbf{y}_t}^{-1}(\xi_i) \tag{2}$$

where $\vec{\nu}_i \in \mathbb{R}^3$. Then, an expectation $\mathbb{E}[\cdot]$ is calculated on the tangent plane $T_{\mathbf{y}_t}\mathbb{S}^2$ and projected back onto $\mathbb{S}^2$ by a projection $\exp_{\mathbf{y}_t}$, i.e.,

$$\mathbf{y}_{t+1} = \exp_{\mathbf{y}_t}\left(\mathbb{E}\left[\{\tilde{\nu}_\mathbf{i}\}_{i=1}^N\right]\right) \tag{3}$$

where $\mathbb{E}\left[\{\tilde{\nu}_\mathbf{i}\}_{i=1}^N\right] = \left(\frac{1}{N}\sum_1^N \nu_{1,i}, \frac{1}{N}\sum_1^N \nu_{2,i}, \frac{1}{N}\sum_1^N \nu_{3,i}\right)$.

For the unit sphere $\mathbb{S}^2$, with the Riemannian metric induced by the Euclidian metric on $\mathbb{R}^3$, the inverse exponential map (or logarithmic map) is given by [2]

$$\exp_{\mathbf{y}}^{-1}(\xi) = [1 - (\mathbf{y}\cdot\xi)^2]^{-1/2}(\xi - (\mathbf{y}\cdot\xi)\mathbf{y}))\arccos(\mathbf{y}\cdot\xi) \tag{4}$$

where $\mathbf{y}, \xi \in \mathbb{S}^2$. The explicit expression for the exponential map is [2]

$$\exp_{\mathbf{y}}(\vec{\nu}) = \cos(\|\vec{\nu}\|)\mathbf{y} + \sin(\|\vec{\nu}\|)\frac{\vec{\nu}}{\|\vec{\nu}\|} \tag{5}$$

where $\vec{\nu} \in T_{\mathbf{y}}\mathbb{S}^2$ and $\vec{\nu} \neq (0,0,0)$.

Using t as an iteration index, Eq. (2) and (3) leads to a gradient descent iterative algorithm Choosing an appropriate starting point $\mathbf{y}_0$ the algorithm converges within a few iterations to the Fréchet mean: $\mathbf{y}_T = \mu^{\circ}(R)$ such that $\mathbf{y}_{T+1} = \mathbf{y}_T$.

3. SUPREMUM AND INFIMUM ON $\mathbb{S}^2$

Algorithms to determine supremum and infimum values for a set of points lying on $\mathbb{S}^2$ are introduced in this section. They are applied to the corresponding sup and inf operators found in the definitions of dilation and erosion, which lead to pseudo-dilation and pseudo-erosion for image valued on $\mathbb{S}^2$.

Supremum. Let $R = \{\xi_i\}_{i=1}^N$ be a set of points lying on the sphere surface. First, the Fréchet mean of the set is computed, as explained in Section 2: $\bar{\xi} = \mu^{\circ}(R)$. Considering this center as the origin of R, we use it to carry out a rotation on $\mathbb{S}^2$ of each point belonging to the set R. The barycenter is moved to the "north pole", $\mathbf{N} = (0,0,1)$, and this translation completely describes the axis and the angle needed to determine the rotation matrix $\mathcal{M}_{\mathbf{N}}(\bar{\xi})$, which is then applied to all the points for the points of R:

$$\xi_i \mapsto \tilde{\xi}_i = \mathcal{M}_{\mathbf{N}}(\bar{\xi}) \cdot \xi_i^T \quad \forall \xi_i \in R \tag{6}$$

where T is the transpose operator and $\tilde{}$ indicates the location coordinates once rotated. Therefore, all $\tilde{\xi}_i \in \tilde{R}$ and $\tilde{\bar{\xi}} = (0,0,1)$, the previously computed Fréchet mean, are placed around $\mathbf{N}$, preserving the same configuration they had, see Fig. 2.

Next step, all $\tilde{\xi}_i \in \tilde{R}$ will be projected to the space tangent at $\mathbf{N}$, denoted $T_{\mathbf{N}}\mathbb{S}^2$, using the expression referred in Eq. (4). Let us denote by $\vec{\nu}_i = (\nu_{1,i}, \nu_{2,i}, \nu_{3,i})$ are the projected points on $T_{\mathbf{N}}\mathbb{S}^2$:

$$\vec{\nu}_i = \exp_{\tilde{\bar{\xi}}}^{-1}(\tilde{\xi}_i) \tag{7}$$

Thus, having $\mathbf{N} = (0,0,1)$ as the projection point leads to a tangent plane contained in $\mathbb{R}^2$, i.e., $T_{\mathbf{N}}\mathbb{S}^2 \subset \mathbb{R}^2$ such that $\nu_{3,j} = 0, \forall j$. The smallest box that may contain these points in $T_{\mathbf{N}}\mathbb{S}^2$ is defined by its four corners, obtained as the minimum and maximum values of each of the coordinates for both axes, and the combinations between them, i.e., $\vee\nu_{1,i}$, $\wedge\nu_{1,i}$ and $\vee\nu_{2,i}$, $\wedge\nu_{2,i}$, see Fig. 1. We consider these four points as the four candidates to calculate the supremum:

$$\vec{\nu}_{sup} \in \{\vec{\nu}_1^{\square} = (\vee\nu_{1,i}, \vee\nu_{2,i}), \vec{\nu}_2^{\square} = (\wedge\nu_{1,i}, \wedge\nu_{2,i}),$$
$$\vec{\nu}_3^{\square} = (\vee\nu_{1,i}, \wedge\nu_{2,i}), \vec{\nu}_4^{\square} = (\wedge\nu_{1,i}, \vee\nu_{2,i})\}$$

Then, we select as supremum the one furthest from $\tilde{\bar{\xi}}$. As $\tilde{\bar{\xi}}$ in tangent space $T_{\mathbf{N}}\mathbb{S}^2$ corresponds to the origin $(0,0)$, it is equivalent to say that $\vec{\nu}_{sup}$ is the corner of the box having the largest norm, i.e.,

$$\vec{\nu}_{sup} = \underset{j=1,\cdots,4}{\arg\max} \|\vec{\nu}_j^{\square}\| \tag{8}$$

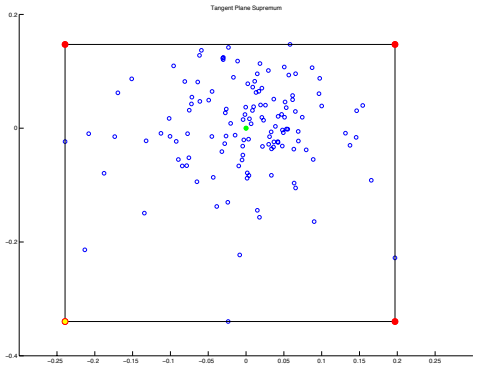

Fig. 1. Tangent plane $T_{\mathbf{N}}\mathbb{S}^2$, with all the projected points $\vec{\nu}_i$. We note that $\tilde{\bar{\xi}}$, in green, is found at the origin. The red dots are the four candidates $\vec{\nu}_j^{\square}$, $j = 1, \cdots, 4$, and the yellow one is the furthest from the origin $\vec{\nu}_{sup}$.

Now, $\vec{\nu}_{sup}$ is projected back to the sphere, according to Eq. (5):

$$\tilde{\xi}_{sup} = \exp_{\tilde{\bar{\xi}}}(\vec{\nu}_{sup}) \tag{9}$$

and finally moved to its corresponding location by reversing the rotation:

$$\overset{\circ}{\underset{\bar{\xi}}{\sup}}\left[\{\xi_i\}_{i=1}^N\right] = \mathcal{M}_{\mathbf{N}}(\bar{\xi})^T \cdot \tilde{\xi}_{sup}^T \tag{10}$$

An example of the complete algorithm is given in Fig. 2.

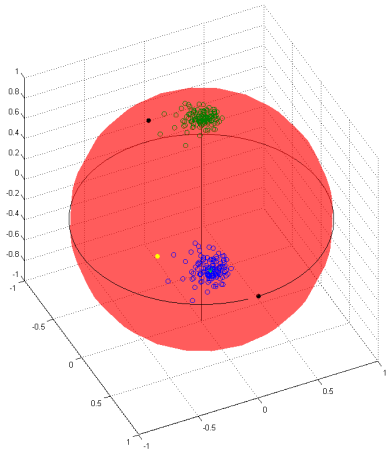

Fig. 2. Original set R of points (in blue), and its Fréchet mean in green. The result of the rotation of the set to $\mathbf{N}$ and how $\vec{\nu}_{sup}$ is projected back to the sphere and the rotation is reversed, in yellow the value of the supremum.

Infimum. The method proposed to calculate the infimum is similar to the one presented for the supremum. In fact, we

will introduce a duality in $T_{\mathbf{N}}\mathbb{S}^2$ which is associated to the inversion of coordinates.

We start by the same steps as for the supremum: after computing the Fréchet mean Eq.(3), and performing the rotation of the set Eq.(6), all $\tilde{\xi}_i \in \tilde{R}$ are projected to the plane tangent at $\mathbf{N}$ using Eq.(7).

Now, the coordinates of each $\vec{\nu}_i$ lying on $T_N\mathbb{S}^2$ are inverted to obtain a set of point given by

$$\vec{\theta_i} = \left(\frac{1}{\nu_{1,i}}, \frac{1}{\nu_{2,i}}, 0\right) \tag{11}$$

Computing the maximum and minimum for inverted coordinates $\theta_{1,i}$ and $\theta_{2,i}$, $i = 1 \cdots N$, it is obtained, as for the supremum, the four candidates to the infimum:

$$\vec{\theta}_{inf} \in \{\vec{\theta}_1^{\square}, \vec{\theta}_2^{\square}, \vec{\theta}_3^{\square}, \vec{\theta}_4^{\square}\}$$

where

$$\vec{\theta}_1^{\square} = \left(\bigvee \frac{1}{\nu_{1,i}}, \bigvee \frac{1}{\nu_{2,i}}\right), \quad \vec{\theta}_2^{\square} = \left(\bigwedge \tfrac{1}{\nu_{1,i}}, \bigwedge \tfrac{1}{\nu_{2,i}}\right)$$
$$\vec{\theta}_3^{\square} = \left(\bigvee \frac{1}{\nu_{1,i}}, \bigwedge \frac{1}{\nu_{2,i}}\right), \quad \vec{\theta}_4^{\square} = \left(\bigwedge \tfrac{1}{\nu_{1,i}}, \bigvee \tfrac{1}{\nu_{2,i}}\right)$$

and the one furthest from the Fréchet mean is chosen:

$$\vec{\theta}_{inf} = \underset{j=1,\cdots,4}{\arg\max} \|\vec{\theta}_j^{\square}\| \tag{12}$$

The coordinates of the point $\vec{\theta}_{inf}$ are reinverted to obtain the infimum in original tangent space $T_N\mathbb{S}^2$:

$$\vec{\nu}_{inf} = \left(\frac{1}{\theta_{1,inf}}, \frac{1}{\theta_{2,inf}}, 0\right)$$

and then, $\vec{\nu}_{inf}$ on $T_N\mathbb{S}^2$ is projected back onto the sphere:

$$\tilde{\xi}_{inf} = \exp_{\bar{\xi}}(\vec{\nu}_{inf}) \tag{13}$$

In the last step, the infimum for R is obtained once the rotation is undone:

$$\overset{\circ}{\underset{\bar{\xi}}{\inf}} \left[\{\xi_i\}_{i=1}^N\right] = \mathcal{M}_{\mathbf{N}}(\bar{\xi})^T \cdot \tilde{\xi}_{inf}^T \tag{14}$$

It may be mentioned that when including all the points in a rectangular box, an extension of 2D Euclidean balls is conducted. The corresponding boxes conform the minimum solid angle including all the points for the supremum and the maximum solid angle including just the Fréchet mean for the infimum. Although the physical meaning is unclear, it is worth indicating the geometric consistency with classical topology definitions.

Definition of sup/inf-based operators. Given an image valued on the sphere $f(x,y) \in \mathcal{F}(E,\mathbb{S}^2)$, we introduce the *flat pseudo-dilation on the sphere* as the operator defined by

$$\begin{cases} \delta^{\circ}_{W,B}(f)(x,y) = \left\{\sup^{\circ}_{\bar{\xi}}\left[f(u,v) = \xi_j\right], (u,v) \in B(x,y)\right\} \\ \\ \text{with } \bar{\xi} = \mu^{\circ}\left(\left[f(n,m) = \xi_i\right]\right), (n,m) \in W(x,y) \end{cases} \tag{15}$$

where B defines the shape of the structuring element and W is the window used for computing the Fréchet mean $\bar{\xi}$. Similarly, the *flat pseudo-erosion on the sphere* is defined by

$$\begin{cases} \varepsilon^{\circ}_{W,B}(f)(x,y) = \left\{\inf^{\circ}_{\bar{\xi}}\left[f(u,v) = \xi_j\right], (u,v) \in \check{B}(x,y)\right\} \\ \\ \text{with } \bar{\xi} = \mu^{\circ}\left(\left[f(n,m) = \xi_i\right]\right), (n,m) \in W(x,y) \end{cases} \tag{16}$$

They are referred as "pseudo-dilation" (resp. "pseudo-erosion") because, although its behavior is intuitively coherent with the classical dilation (resp. erosion), they are not fully equivalent. More precisely, the distributivity and associativity properties are not satisfied for the operators (15) and (16) described above. These limitations are well known for the "locally adaptive" operators [7]; we note that here the adaptavility appears in the computation of the local origin.

4. APPLICATION OF MORPHOLOGICAL PROCESSING ON $\mathbb{S}^2$

Using the pseudo-dilation and pseudo-erosion on the sphere as basic bricks, other derived morphological operators can be extended to images valued on the sphere. Using the proposed formulations on the sphere for pseudo-dilation (15) and pseudo-erosion (16), we define the *morphological gradient on the sphere* of image $f \in \mathcal{F}(E,\mathbb{S}^2)$ as their difference image: $g^{\circ}_{W,B}(f)(x,y) = d\left(\delta^{\circ}_{W,B}(f)(x,y), \varepsilon^{\circ}_{W,B}(f)(x,y)\right)$, where $d(\xi_i,\xi_j)$ is the Riemannian distance on $\mathbb{S}^2$. In mathematical morphology, opening and closing are two key transformations for filtering purposes, both derived from erosion and dilation by their direct products. Now, using the corresponding expressions detailed on the sphere, we shall define the *flat pseudo-opening on the sphere* of an image $f \in \mathcal{F}(E,\mathbb{S}^2)$ as the flat pseudo-dilation (15) applied on the resulting pseudo-erosion (16) of the original image f, i.e., $\gamma^{\circ}_{W,B}(f) = \delta^{\circ}_{W,B}\left(\varepsilon^{\circ}_{W,B}(f)\right)$. Similarly, the *flat pseudo-closing on the sphere* is defined as $\varphi^{\circ}_{W,B}(f) = \varepsilon^{\circ}_{W,B}\left(\delta^{\circ}_{W,B}(f)\right)$. The interpretation of these operators is exactly the same as for the opening/closing of grey-level images: opening removes objects from the foreground smaller than the structuring element and closing eliminates small holes in the background. Once the pseudo-opening and pseudo-closing on the sphere have been well-defined, we can also generalize the corresponding residue-based operators. Indeed the *white top-hat on the sphere* is the residue between the original image and its pseudo-opening transformation: $\rho^{+,\circ}_{W,B}(f)(x,y) = d\left(f(x,y), \gamma^{\circ}_{W,B}(f)(x,y)\right)$. Similarly, the *black top-hat on the sphere* is the residue between the original image and its pseudo-closing. As for the grey-level case, the white (resp. black) top-hat allows extracting the image structures which have been removed by the opening (resp. the closing).

For the examples given in Fig. 3, each pixel denotes a polarization state (ie., a point lying on the sphere surface) or

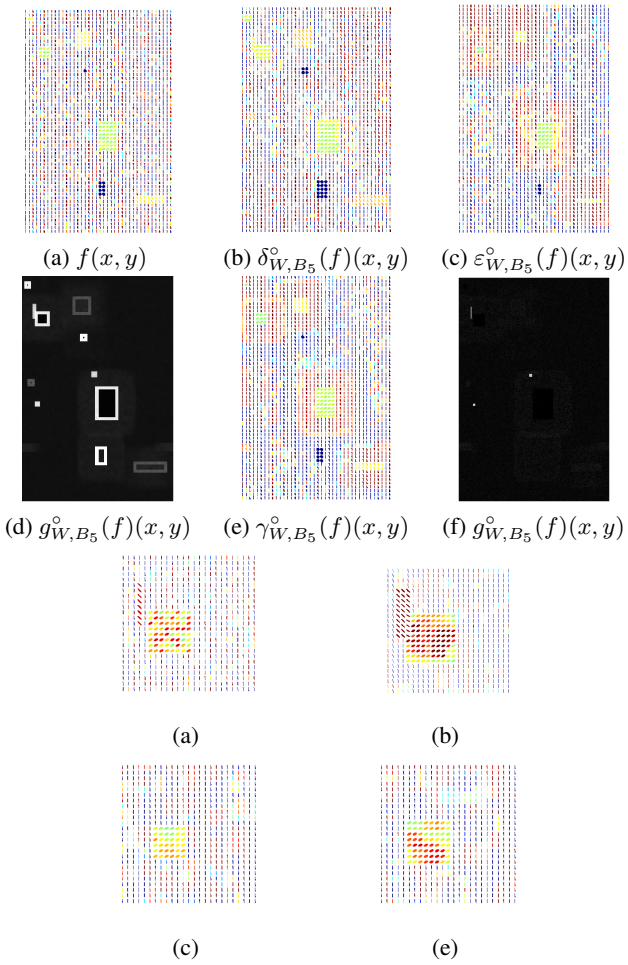

Fig. 3. Top, examples of pseudo-dilation (b), and pseudo-erosion (c), of image $f(x,y) \in \mathbb{S}^2$, given in (a), and its derived morphological operators. Bottom, zoomed-in part of images. The structuring element B_n is a square of 5×5 pixels and W is a square of 55×55. Note that for the gradient and the top-hat images, the result is the given scalar image.

more generally an ellipsoid describing the distribution of gradient directions. We point out that the performance of the described operators remains consistent with the definitions for a grey-level image.

5. CONCLUSIONS AND PERSPECTIVES

We have explored a novel approach to the computation of supremum and infimum of a set of points on $\mathbb{S}^2$, which is based on the notion of local origin to obtain the best tangent space where the supremum and infimum are computed as a vector notion. This methodology seems interesting from a practical viewpoint since the obtained morphological filters produce useful results. There are some questions which should be explored in detail in subsequent studies. On the one hand, it should be proved that this local approach is more appropriate than a global one, typically computing the supremum and infimum in the space associated to the stereographic projection. On the other hand, there are some limited invariance properties of the supremum and infimum which are due to the computation in a rectangular box. It seems more interesting to consider a Euclidean ball (i.e., the supremum can be the point of the minimum enclosing ball which have the largest norm). A deeper study on the mathematical properties of the proposed pseudo-dilation and pseudo-erosion is also required.

6. REFERENCES

[1] S.R. Buss, J.P. Fillmore. *Spherical averages and applications to spherical splines and interpolation.* ACM Transactions on Graphics, 20: 95–126, 2001.

[2] P.T. Fletcher, S. Venkatasubramanian, S. Joshi. *Robust Statistics on Riemannian Manifolds via the Geometric Median.* In Proceedings of CVPR'08, 2008.

[3] S. Fiori. *On vector averaging over the unit hypersphere.* Digital Signal Processing, 19:715–725, 2009.

[4] M. Fréchet. *Les élements aléatoires de nature quelconque dans un espace distancié.*Ann. Inst. H. Poincaré, 10: 215–310, 1948.

[5] A. Hanbury, J. Serra. *Morphological Operators on the Unit Circle.* IEEE Transactions on Image Processing, 10(12):1842–1850, 2001.

[6] H. Karcher. *Riemann center of mass and mollifier smoothing.* Communications on Pure and Applied Mathematics, 30: 509–541, 1997.

[7] J. Roerdink. *Adaptivity and group invariance in mathematical morphology.* In Proc. of IEEE International Conference on Image Processing (ICIP'09), pp. 2253–2256, 2009.

[8] J. Serra. *Image Analysis and Mathematical Morphology, Vol I.* Academic Press, NY, London, 1982.

[9] J. Serra. *Anamorphoses and Function Lattices (Multivalued Morphology).* In (Dougherty, Ed.) Mathematical Morphology in Image Processing, Marcel-Dekker, 483–523, 1992.

[10] P. Soille. *Morphological Image Analysis.* Springer-Verlag, Berlin, 1999.

[11] S. Velasco-Forero, J. Angulo. *Supervised ordering in R^n: Application to morphological processing of hyperspectral images.* IEEE Transactions on Image Processing, 20(11): 3301–3308, 2011.

[12] Y. Wang, C. Han. PolSAR Image Segmentation by Mean Shift Clustering in the Tensor Space. In *Acta Automatica Sinica* 36: 798–806, 2010.

[13] http://www.ceremade.dauphine.fr/ peyre/matlab/diffc/content.html#3